

# PARAMETRIC STUDY OF THE 3D ICE BLOCK TRAJECTORIES AROUND A WING

**Hassan EL Sahely**

Department of Mechanical Engineering,  
École de Technologie Supérieure,  
Montréal, Canada H3C 1K3,  
[hassan.el-sahely.1@ens.etsmtl.ca](mailto:hassan.el-sahely.1@ens.etsmtl.ca)

**Francois Morency**

Department of Mechanical Engineering,  
École de Technologie Supérieure,  
Montréal, Canada H3C 1K3,  
[francois.morency@etsmtl.ca](mailto:francois.morency@etsmtl.ca)

## ABSTRACT

*Ice accretion may occur on unprotected surfaces while an aircraft is flying in the saturated vapor clouds. It may cause a fatal degradation of the wing lifting and handling capabilities. Trying to protect the wing by detaching the ice from the leading edge will cause the appearance of a new problem: the unknown trajectories of the detached ice pieces. Those ice pieces transform into a flying hazard that can cause serious damage to the aircraft engines installed on the rear part of the fuselage. Numerical studies, for example using CFD, are available in the literature(Ignatowicz, Morency, & Lopez, 2019) over specific domains. The ice pieces fly into a discretized domain where velocity are known at mesh nodes. The velocities at specific ice piece locations are first obtained by interpolation of the CFD velocity between nodes and then the drag force is computed. If several geometries are to be studied, CFD requires multiple meshes, thus increasing the computation time. To avoid the 3D mesh generation time, this paper aims to computes trajectories around a wing using a 3D panel method that requires only a coarse surface mesh of the wing surface. It is assumed that viscous effects near aircraft surface play a negligible role on the ice piece trajectory. Panel methods do not need volume mesh in the domain around the wing, which speed up the computing time of the flow and ease the task of parametric studies of the wing shape effects on trajectory. This advantage is absent in other studies using CFD mesh that takes large computation time. A modified version of an existing 3D panel code (adding wing tip patch and add velocity computation) is developed to enable the trajectories study. First, the results show a verification cases for the modified panel method. Moreover, a comparison with the literature cases will be illustrated for one trajectory around an infinite and a finite wing. Then, the effect of sweepback angle on the ice shedding as well as trajectories will be held, using a Monte-Carlo statistical approach. The probability function for the passage of an ice piece follow a bi-normal law, on the z-axis.*

**Keywords:** Trajectories, 3D Panel Method, Ice-shedding, Hazard, Computation, Monte-Carlo.

## Abbreviation

3DPM : 3D panel Method

CFD : Computational fluid dynamics

BWB : Blended wing body

$\theta$	: Pitch angle
$\psi$	: Rolling angle
$\phi$	: Yawing angle
DOF	: Degree of freedom

## INTRODUCTION

Flying in saturated clouds below freezing points is potentially dangerous for aircraft. The icing conditions can have severe effects on the aircraft having problems with their anti-icing system. Ice protection systems, especially on the leading edge, are responsible for preventing ice accumulation, and therefore preventing incidence or even crash. Ice accretion will cause severe damages of the aircraft aerodynamic capabilities, which decrease lift by reducing the stall angle of attack and increase the parasite drag due to wing camber transformation and roughness. Systems are proposed to remove the accumulated ice on the wing leading edge (Thomas et al., 1996). For example, special membrane that can be inflated and detach the ice can be added. The trajectories of the detached ice particles are unknown because of their unpredictable sizes and shapes. This problem can be studied either experimentally in the wing tunnel or numerically by computer code. Specific shapes for the shed ice-pieces are needed, like spheres and flat plates, to eases the task for experimental and numerical computation of the trajectories.

Ignatowicz et al., (2019) studied the trajectories around a BWB aircraft by proposing a 3D dynamic moment on the flat plate. Ignatowicz took the 2D dynamic moment of Tachikawa (1983) and extend it into 3D model. Papadakis et al. (2007) performed Monte-Carlo simulations with 30,000 trajectories of ice particles detached from wing using CFD. They studied the percentage of ice-particle hit on the aircraft body, wing and the engine mounted on the fuselage. Santos, Papa, et Do Areal Ferrari (2003) proposed a simulation model in Fluent to evaluate the risk of the ice impact on a NACA based wing. This model simulates the region of impact after the wing at X=8m, at span section y=0.1 m from the wing to 5m up. But they used a low number of ice particle trajectories which is 343 ice-pieces.

This paper present a study of the trajectories around a rectangular wing based on NACA0012 airfoil. Although all the previous studies used a CFD flow field (Ignatowicz et al., 2019; Papadakis, Yeong, & Suares, 2007), this study is based on a 3D potential based panel method (Katz & Plotkin, 2001)to estimate the flow field around the wing. Moreover, the effect of sweepback angle and taper ratio is held. The final step presents a Monte-Carlo approach which illustrate the effect of the trajectories on the probability map. Monte-Carlo simulation shows that the probability map of the trajectory's footprint will be a normal distribution along the y-axis and binormal along the x-axis.

In this paper, a mathematical model of the problem is illustrated, then a proposed method to close the wing tip patch to correct the flow around the wing. Also, the method used in obtaining the 3D trajectories with 6 DOF is explained. Next a verification case of the method against CFD and against the commercial software XFLR5 are held. Finally, a Monte-Carlo study is done in order to show the probability distribution after simulating many cases varying the number of trajectories.

## MATHEMATICAL MODELING

The method used to compute trajectories are based on a 3DPM. This method can provide the correct flow field around the wing. It allows to compute the velocity anywhere in the near and farfield as a preparation for trajectory computation. This method is explained in the next three sections and in details in the ANNEX1.

### 3D Panel method

Let's consider a uniform flow, having a wake and the farfield flow is incompressible, inviscid and irrotational. The potential flow around the solid body is defined by the perturbation potential velocity and the uniform velocity as the following:

$$\Phi = \phi + \Phi_\infty \quad (1)$$

where,

$$\Phi_\infty = U_\infty x + V_\infty y + W_\infty z \quad (2)$$

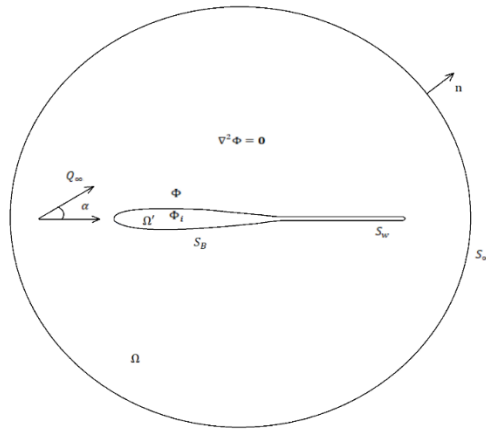


Figure 1. potential flow around a solid body

As the aim is to solve the velocity of the flow field, the Laplace equation is stated as follows:

$$\nabla^2 \Phi = 0 \quad (3)$$

Equation (3) is solved assuming 3 boundary conditions:

- Firstly, the velocity vector component which is normal to the solid boundaries of the airfoil must be zero:

$$\nabla \Phi \cdot n = 0 \quad (4)$$

- Secondly, the disturbance induced will decay away from the solid body as:

$$\lim_{r \rightarrow \infty} \nabla \Phi = Q_\infty \quad (5)$$

- Thirdly, the solution should satisfy the Kutta-condition at the trailing edge of the lifting body such that the potential jump across the wake surface  $S_w$  is the same as the circulation  $\Gamma$ .

$$[\Delta\Phi]_{on\ S_w} = \Gamma = constant = \Delta\Phi_{T.E.} \quad (6)$$

### Velocity calculation in the farfield

With the source and doublet element at each panel from previous calculation, Katz & Plotkin (2001) identified a way to calculate the point source and doublet influence respectively for the velocity potential mentioned above, by the following:

$$\text{For source: } \Phi_{(x,y,z)} = \frac{-\sigma A}{4\pi\sqrt{(x-x_0)^2+(y-y_0)^2+z^2}} \quad (7)$$

$$\text{For doublet: } \Phi_{(x,y,z)} = \frac{-\mu A.z}{4\pi\sqrt[3]{(x-x_0)^2+(y-y_0)^2+z^2}} \quad (8)$$

where,  $\sigma$  is the source element,  $\mu$  is the doublet element,  $A$  is the panel area,  $x, y, z$  are the coordinate of the point of interest in the farfield,  $x_0, y_0, z_0$  are the collocation point coordinate of the panel.

The velocity components due to the source ( $u_s, v_s, w_s$ ) and doublet element ( $u_d, v_d, w_d$ ), are obtained by differentiating the equations (7) and (8) with respect to  $x, y, z$  respectively. Then, those three velocity components will be added to the flow velocity components to form the total velocity:

$$\begin{aligned} u_{total} &= u_s + u_d + Ut \\ v_{total} &= v_s + v_d + Vt \\ w_{total} &= w_s + w_d + Wt \end{aligned} \quad (9)$$

where,  $Ut$ ,  $Vt$  and  $Wt$  are the free stream velocity components in  $x, y, z$  direction respectively.

### Closing wing tip

The wing presented in this calculation has 5(m) of span and 1(m) of chord and has an open end on the tip as defined in Katz & Plotkin (2001). The mesh discretization is mentioned on the ANNEX 1. The next section present an algorithm on how to close the wing tip. New corner points are added, in the center of the tip plane along the chord. This will form new panels at the tip. Then, the collocation points are calculated in the middle of the new panels. At the joint point the first counter point and the last point are in the same location. It seems to be a triangular panel but in fact it is rectangular with two superposed points. After that, the panel parameters are calculated in the collocation points. This closing of the wing tip is needed to obtain the right lift coefficient as well as the flow on the tip.

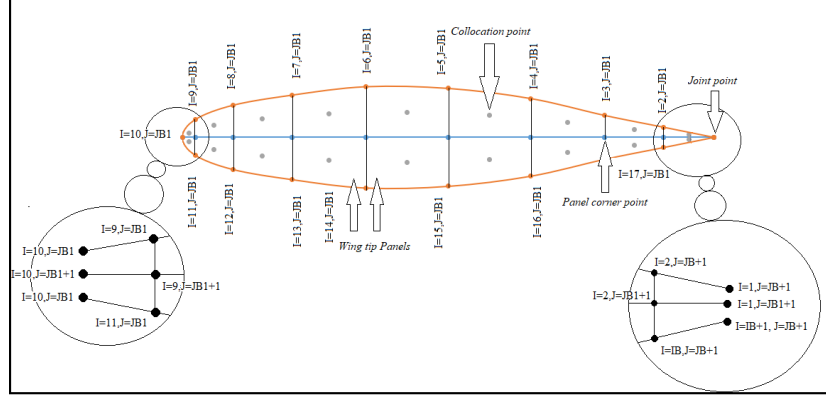


Figure 2. Figure showing the closing wing tip by adding some panels.

### 3D trajectories with 6-DOF.

The particle motion is based on the Newton's second law (Ignatowicz et al,2019). The simulation of the trajectories depends on several conditions: shape of the ice particle (in this case flat plate) and initial conditions. The initial conditions of the particle simulations are the position at which the particle is detached and its initial Euler angles ( $\theta, \psi, \phi$ ) roll, pitch, yaw, respectively with respect to the global frame of reference. When the particle moves after the detachment it rotates. This rotation create moment on the particle. The damping moment is considered as well in this study (Ignatowicz et al.,2019). The methodology will start by computing the flow field velocity at the ice location by the panel method at each time step.

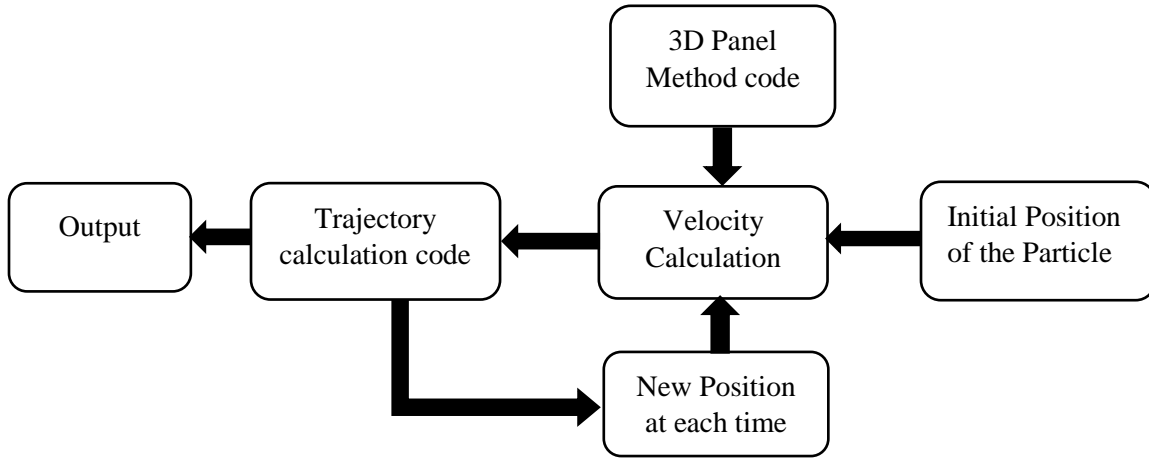


Figure 3. Methodology for computation of the trajectory.

### Monte-Carlo simulation

To simulate the trajectories of ice-piece with uncertainty on the initial condition is a key to be more realistic. The Monte-Carlo simulation are often used in ice shedding studies. When

the ice is detached from the leading edge, it will possess a different initial position and angles that follows distribution probability functions. The parameters vised to be changed are the initial position of the particle and the initial Euler angles (pitching, rolling, yawing). The random initial position of the particle is calculated by the following formula (Shimoji, 2010):

$$P = P_{min} + |Range| \times R \quad (10)$$

where R is a random generator,  $P_{min}$  is the minimum parameter, P is the parameter to be evaluated and Range is the interval of freedom of a parameter.

For the initial-rotation angle, the following formula is used:

$$\theta, \psi, \phi = (R - 0.5) \times Ri(180) \quad (11)$$

where, Ri is a MATLAB function to give random integer angles. The 0.5 in the formula stands for the alternation between -90 and +90.

As for the initial velocity for the coming calculation a fixed value is used:

$$V_i = 0.7R \quad (12)$$

## CFD

For CFD the software used is SU2, the geometry description will be as follows: 3D rectangular wing based on NACA0012 airfoil, a freestream velocity with 1m/s, AOA=0°, chord length=1m, span=1m. The mesh possesses a 5.7 million hexahedral cell. Next figure (4) shows the mesh and the computational domain. This test case is used to verify the 3DPM flow field and CFD flow field.

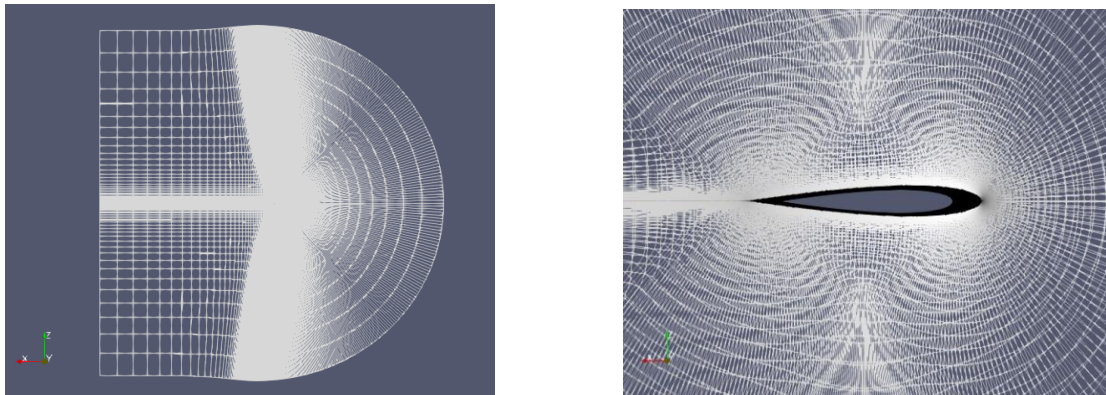


Figure 4. Computational domain of the wing

## Results and discussion

The figure (5) illustrates the lift force coefficient versus the angle of attack. As it's known the inviscid 3DPM predict a lift coefficient having a linear variation with angle of attack

because it doesn't take into consideration the stall phenomenon and deals with incompressible flow. The figure (5) shows the correction of the lift coefficient after closing the wing tip in comparison with the open source software XFLR5 (the website reference in the references section). Figure (6) shows a verification case of the pressure coefficient with respect to the chord. The pressure coefficient obtained from 3DPM is compared against the one obtained from the software XFLR5. The pressure coefficient is calculated on a mesh having 18, 26 and 36 airfoil coordinates chordwise and 5 sections spanwise at the root section.

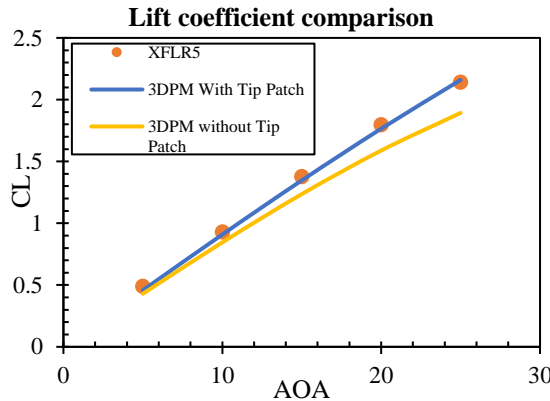


Figure 5. Total lift coefficient comparison.

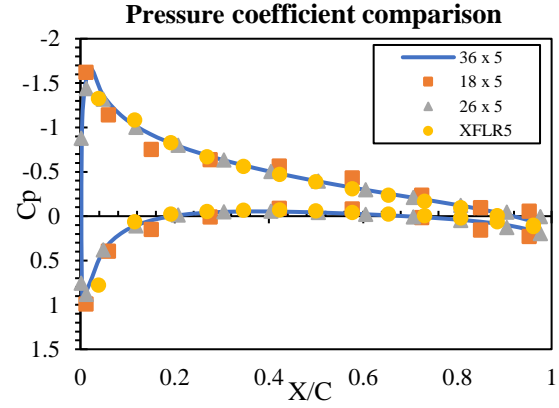


Figure 6. Pressure coefficient at AOA=5

## Trajectory computations

### CFD vs 3DPM

The 3D panel method provide velocity calculations at any point requested in the flow field. Figure (7) shows the pressure coefficient distribution along the chord for 2D airfoil and 3D wing at the middle section. The 3D mesh used in this comparison is an infinite wing. to obtain the behavior of an infinite wing the wingspan is set to be 50(m). The pressure coefficient for the 3D case is picked up at section 25(m) from the root section. Figure (8) shows a comparison of the pressure coefficient at the middle section of a 1(m)-chord wing (NACA0012 airfoil) with 1(m)-span at the middle section at 0 degrees angle of attack. The comparison is held with the CFD solution versus 3DPM solution versus the open software XFLR5. Figure (8) shows a comparison of the pressure coefficient which is obtained from the geometry characteristics explained in the CFD section using CFD, XFLR5 software and 3DPM.

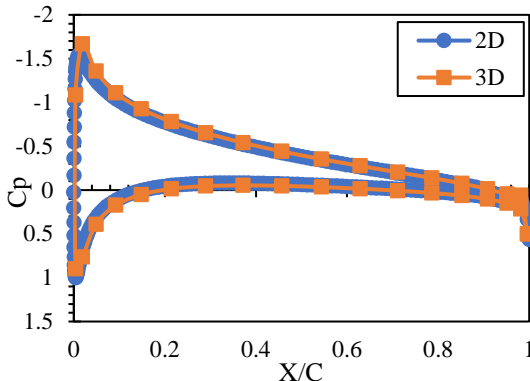


Figure 7. Pressure coefficient comparison at  $\text{AOA} = 5^\circ$

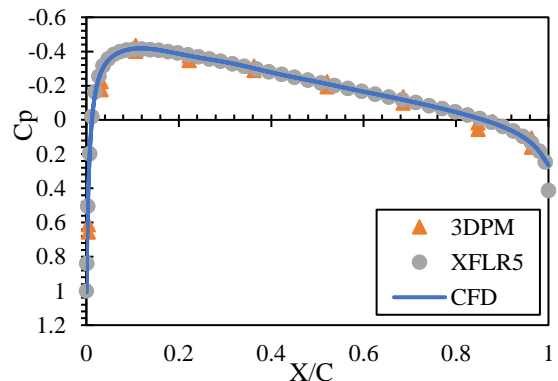


Figure 8. Pressure coefficient comparison at  $\text{AOA} = 0^\circ$

As for the trajectory calculation, the ice particle is chosen to be a flat plate with rectangular shape. Figure (9) and (10) shows an XZ view and YZ view of a trajectory. This test case shows a trajectory shed from the leading edge at 0.5 (m) span. The initial angle of rotation of the ice block is 90 degrees. The dimensions of the ice-piece are 0.2122x0.1601x0.002 (m), the density of the particle 170 kg/m<sup>3</sup> and the air density of 1 kg/m<sup>3</sup>. The comparison presented 7.24% of error is less than 10% which considered acceptable.

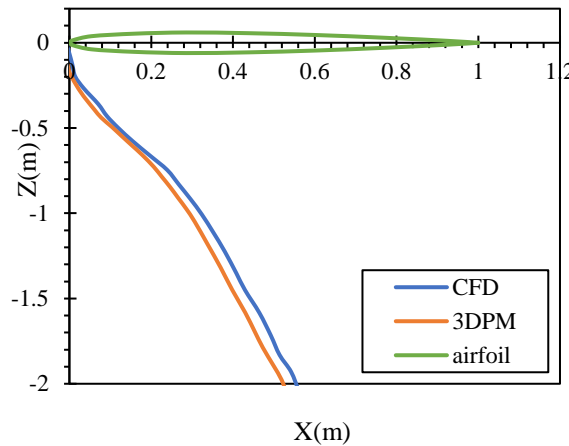


Figure 9. XZ view of the trajectory.

A verification is done against (Suares, 2005) results. Since Suares studied 2D hit trajectories along Z axis, the projection to z axis of the footprint of the particle could be compared to Suares work. Suares simulated 30,000 trajectories and the present code simulated 200 trajectories. The probability map of Suares is done with the following conditions: 3-DOF in

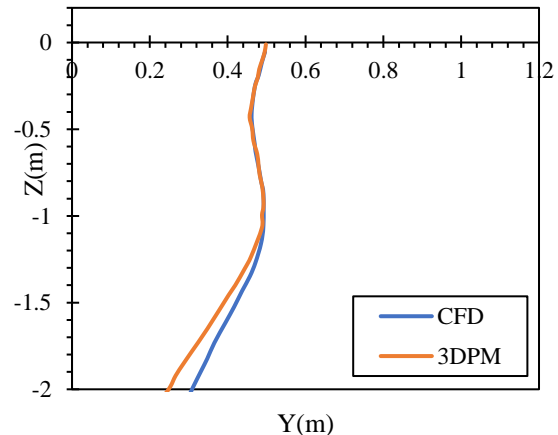


Figure 10. YZ view of the trajectory.

2D airfoil flow field, the flat plat is squared with 0.3(ft) length and 0.025(ft) of thickness. The results are shown in the figure 11. The tendency of the probability distribution along z-axis for both cases (present code and Suares) of the trajectories specially between 2.5 ft and 3.5 ft reaches its maximum hit points at that range.

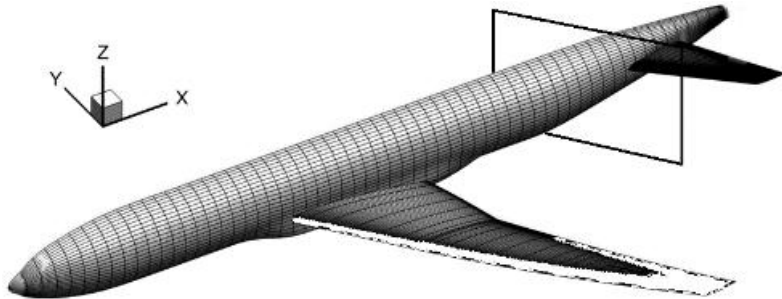


Figure 11. Plane of study after the iced wing (Fujiwara, Nguyen, Livne, & Bragg, 2018)

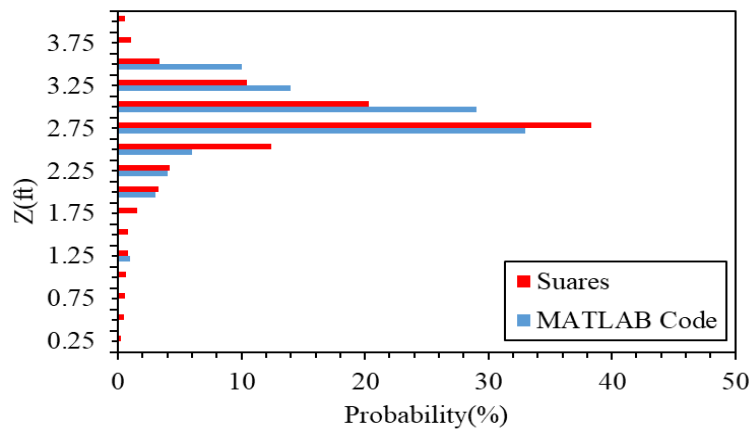
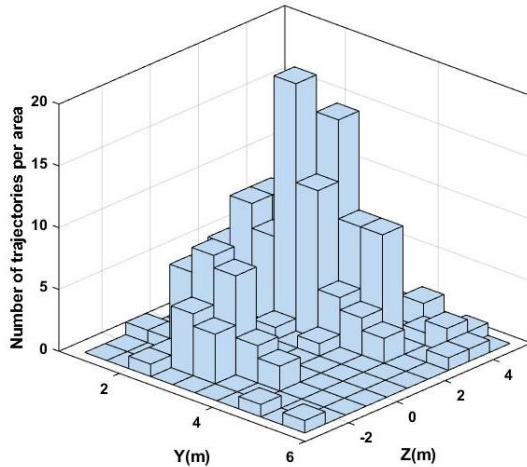


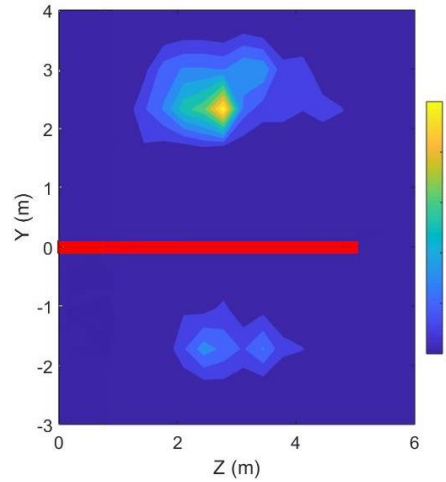
Figure 12. Probability distribution of the trajectories at  $x=2c$  plane behind the wing at AOA = 4 degrees with NACA23012 airfoil.

### Monte-Carlo statistical study

The uncertainty of the statistical study lies on 2 parameters, initial velocity and initial Euler's angles (pitching, rolling and yawing) of the particle. 50, 200, 500 and 1000 trajectories are simulated. The next histogram shows the distribution of the trajectory's footprint per unit area. The study is done using a wing with 5 degrees AOA, 5(m) span, 1(m) chord with zero sweepback angle and taper ratio of 1. The flow field velocity is 220 Knots.



(13a)



(13b)

Figure 13. 3D histogram showing the footprint of the ice-particles at  $x=14$  (ft) for 200 trajectories.

The Monte-Carlo study is done with a large number of trajectories to predict the behavior of the distribution. Previous studies like (Papadakis, Yeong, & Shimoi, 2007) recommended 60,000 trajectories. To reduce computation time, the strategy is to start simulation with a low number of trajectories and then increase the number. This strategy will let to study the behavior of the distribution to know the optimal number of simulations for correct prediction. The figure below shows the probability distribution of the trajectory's footprint for 50, 200, 500 and 1000. For the distribution of the 50 trajectories, shows that the number is not enough since at 200 it changes completely. As the number of trajectories simulated increases, the probability distribution is taking the form of binormal distribution in the z section named  $P(Z)$ . Since  $P(Z)$  is a binormal distribution a study of the behavior of the mean and variance for different number of trajectories is studied. the mean and variance are presented in figure (15) and (16) respectively. Mean 1 and variance 1 represents the trajectory's footprint in the negative side of the z-axis, while mean 2 and variance 2 represents the trajectory's footprint in the positive side of the z-axis.

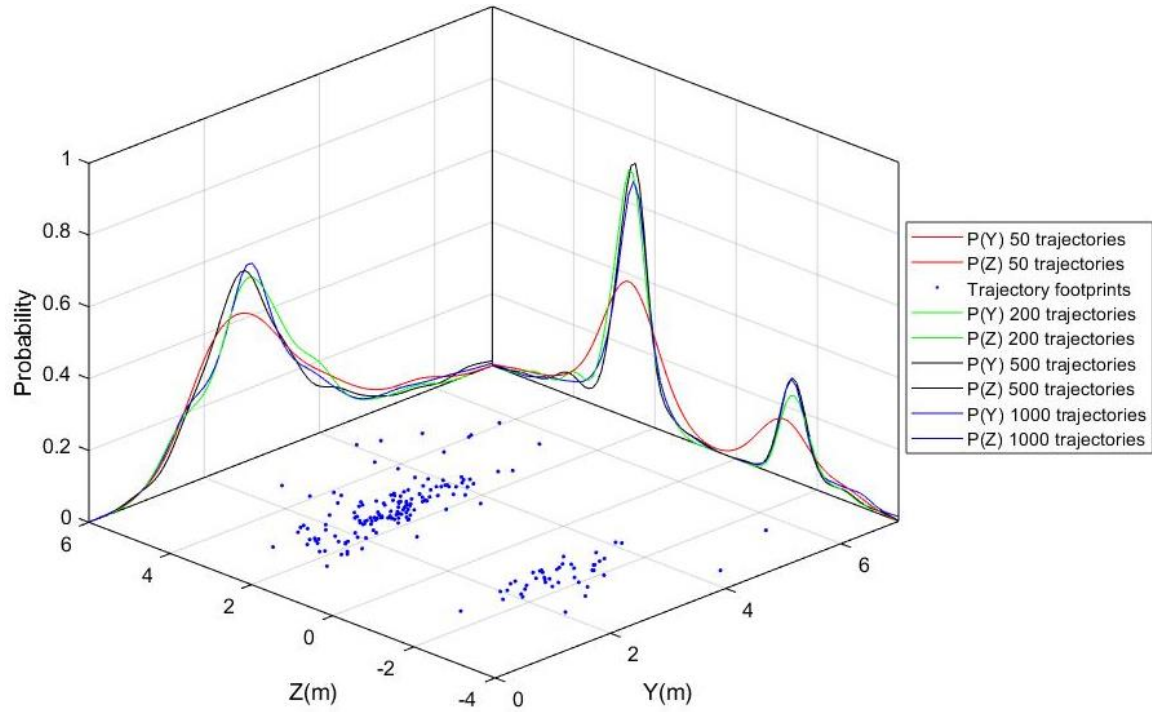


Figure 14. Probability distribution along  $Z$  and  $Y$  axis for 50, 200,500,1000 trajectories.

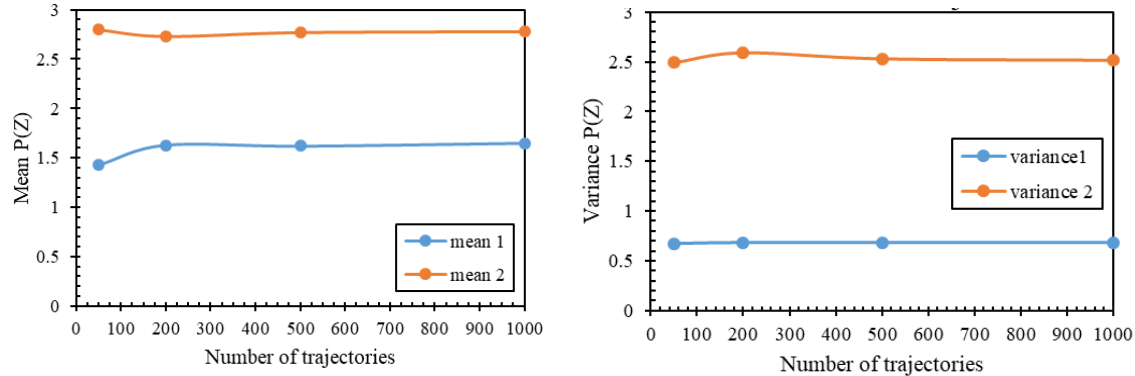


Figure 15. Mean distribution vs number of trajectories.

Figure 16. Variance vs number of trajectories.

The probability distribution function along  $Y$  axis is non-parametric distribution function that takes the form of a Normal distribution. A test is done in the current program (using dfittool function in MATLAB) showed that the distribution fitted the normal one. Similarly, for the distribution along  $z$ -axis, a non-parametric distribution takes the form of a binormal. Figure (15) shows the distribution of the mean with respect to the number of trajectories. Figure (16) shows the variance with respect to the number of trajectories. Next table shows the means and variances for all cases.

Number of Trajectories	50	200	500	1000
mean 1	1.426	1.63	1.62	1.65
mean 2	2.798	2.732	2.773	2.782
variance 1	0.672	0.683	0.682	0.685
variance 2	2.492	2.592	2.532	2.522

Table 1. mean and Variance for different number of trajectories.

### Effect of sweepback angle on the trajectories

The sweepback angle and taper ratio affect the distribution of the particles in a specific plane after the wing. The trajectories cross-section is at 5 (m) after the wing. Figure (17) shows the trajectories footprints in the YZ plane. This test case is done for sweepback angle for 0, 30 and 45 degrees. The trajectories footprint distribution in cross sectional plane shows that by increasing the angle of sweep the trajectories will go toward the aircraft. So as the sweepback angle increase the impact of the trajectories with the aircraft.

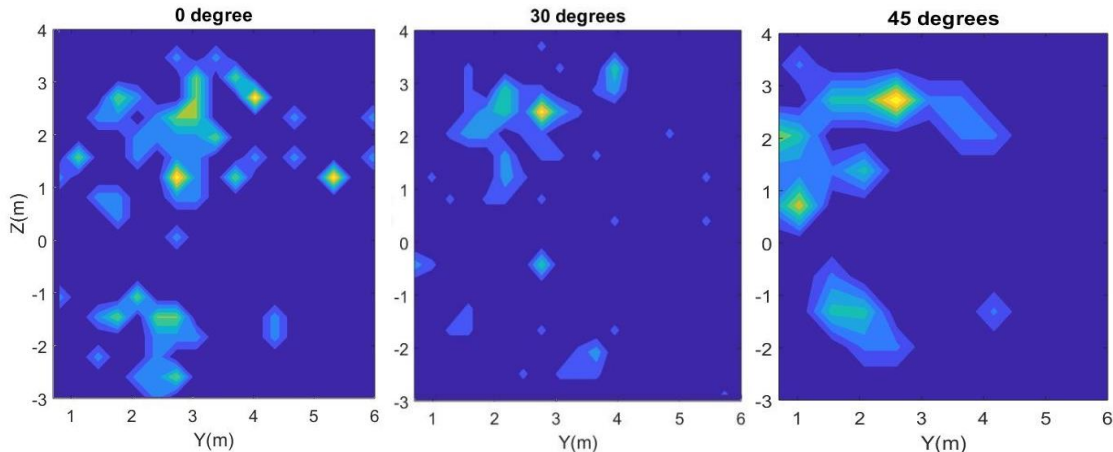


Figure 17. comparison of the footprint location by changing the sweepback angle

### Conclusion

A parametric study of a 3D ice block trajectory is effectuated. A correction of the flow field for the 3DPM was done. The study of the 3DPM methodology in ice-trajectory computation was validated. A comparison of both 3DPM and CFD flow field was stated. The Monte-Carlo study showed that it is not needed to go to very high number of trajectories to predict the shape of the probability distribution of the trajectories.

### References

- Fujiwara, G. E., Nguyen, N. T., Livne, E., & Bragg, M. B. (2018). Aerostructural Design Optimization of a Flexible Wing Aircraft with Continuous Morphing Trailing Edge. Dans *2018 Multidisciplinary Analysis and Optimization Conference* (pp. 3571).

- Ignatowicz, K., Morency, F., & Lopez, P. (2019). Dynamic Moment Model for Numerical Simulation of a 6-DOF Plate Trajectory around an Aircraft. *Journal of Aerospace Engineering*, 32(5), 04019069.
- Katz, J., & Plotkin, A. (2001). *Low-speed aerodynamics* (Vol. 13). Cambridge university press.
- Papadakis, M., Yeong, H.-W., & Shimoi, K. (2007). *Parametric Investigation of Ice Shedding from a Business Jet Aircraft*. SAE Technical Paper.
- Papadakis, M., Yeong, H.-W., & Suárez, I. (2007). Simulation of ice shedding from a business jet aircraft. Dans *45th AIAA Aerospace Sciences Meeting and Exhibit* (pp. 506).
- Santos, L., Papa, R., & Do Areal Ferrari, M. (2003). *A Simulation Model for Ice Impact Risk Evaluation*. doi: 10.2514/6.2003-30
- Shimoi, K. (2010). *Numerical and experimental investigation of ice shedding* (Wichita State University).
- Suárez, I. G. (2005). *Ice particle trajectory simulation* (Wichita State University).
- Tachikawa, M. (1983). Trajectories of flat plates in uniform flow with application to wind-generated missiles. *Journal of Wind Engineering and Industrial Aerodynamics*, 14(1-3), 443-453.
- Tarafder, M. S., Saha, G. K., & Mehedi, S. T. (2010). Analysis of potential flow around 3-dimensional hydrofoils by combined source and dipole based panel method. *Journal of Marine Science and Technology*, 18(3), 376-384.
- Andre Deperrois (2018) XFLR5, Documentation version 6.43.

## ANNEXE I

### Solution by Green's identity

The three-dimensional flow is considered around the wing. The previous Laplace equation can be solved in a three-dimensional domain  $\Omega$ . A boundary  $S$  is divided into  $S_B$ ,  $S_w$ ,  $S_\infty$ . The vector normal  $n$  is always pointing outside the region of interest. Taking a random point  $P$  with coordinates  $(x, y, z)$  away from a singular point  $q (\xi, \eta, \zeta)$  with a distance  $r$  between them. This domain is shown in the figure (1).

Thus (Katz & Plotkin, 2001):

$$\Phi(P) = \frac{1}{4\pi} \int \left[ \frac{1}{r} \nabla(\Phi - \Phi_i) - (\Phi - \Phi_i) \nabla \frac{1}{r} \right] \cdot n \, dS - \frac{1}{4\pi} \left[ \Phi n \cdot \nabla \frac{1}{r} \, dS + \Phi_\infty(P) \right] \quad (1.1)$$

The difference between the internal and external potentials and the difference between their derivatives are respectively as follows (Katz & Plotkin, 2001):

$$-\mu = \Phi - \Phi_i \quad (1.2)$$

$$-\sigma = \frac{\partial \Phi}{\partial n} - \frac{\partial \Phi_i}{\partial n} \quad (1.3)$$

where  $\mu$  and  $\sigma$  are the doublet and source respectively. The minus sign is a result of the normal vector  $n$  pointing into  $S_B$ . In this case, equation (1.13) can be re-written as (Katz & Plotkin, 2001):

$$\Phi(p) = -\frac{1}{4\pi} \int_{S_B} \left[ \sigma \frac{1}{r} - \mu \frac{\partial}{\partial n} \frac{1}{r} \right] dS + \frac{1}{4\pi} \int_{S_w} \left[ \mu \frac{\partial}{\partial n} \frac{1}{r} \right] dS + \Phi_\infty(p) \quad (1.4)$$

### Dirichlet boundary condition

As part of specifying deeper the problem, the boundary conditions are set with respect to Dirichlet problem. He said that the perturbation potential in the  $S_B$  should be specified and the zero-flow normal to the surface is to be specified in terms of velocity potential as follows (Tarafder, Saha, & Mehedi, 2010):

$$\Phi_i = (\phi + \Phi_\infty)_i = const \quad (1.5)$$

The inner potential  $\Phi_i$  with respect to the point  $P (x, y, z)$  inside the surface  $S_B$  is obtained from (1.16) (Tarafder et al., 2010):

$$\Phi_i(P) = \frac{1}{4\pi} \int_{S_B + S_W} \left[ \mu \frac{\partial}{\partial n} \frac{1}{r} \right] dS - \frac{1}{4\pi} \int_{S_B} \left[ \sigma \frac{1}{r} \right] dS + \Phi_\infty \quad (1.6)$$

Pointing out that when  $r \rightarrow 0$ , both integrals will tend to singularity, and near this value the integrals must be evaluated. The boundary inside the solid body is (Tarafder et al., 2010):

$$\frac{1}{4\pi} \int_{S_B + S_W} \left[ \mu \frac{\partial}{\partial n} \frac{1}{r} \right] dS - \frac{1}{4\pi} \int_{S_B} \left[ \sigma \frac{1}{r} \right] dS + \Phi_\infty = const \quad (1.7)$$

The equation (1.23) is very important since we can discretize the solid body into  $N$  panels and the integration for each panel is done by such formula:

$$\frac{1}{4\pi} \sum_{j=1}^N \int_{S_B + S_W} \left[ \mu \frac{\partial}{\partial n} \frac{1}{r} \right] dS - \frac{1}{4\pi} \sum_{j=1}^N \int_{S_B} \left[ \sigma \frac{1}{r} \right] dS + \Phi_\infty = const \quad (1.8)$$

In the panel element, the integration is limited. But it's necessary to mention the influence of panel  $j$  at a random point  $P$  is computed in function of doublet and source respectively as (Tarafder et al.,2010):

$$\begin{aligned} \frac{1}{4\pi} \int_{S_B + S_W} \left[ \frac{\partial}{\partial n} \frac{1}{r} dS \right]_j &\equiv C_j \\ - \frac{1}{4\pi} \int_{S_B} \left[ \frac{1}{r} dS \right]_j &\equiv B_j \end{aligned} \quad . \quad (1.9)$$

Finally, the boundary condition inside the surface allow us to create  $N$  linear equation based on  $N$  collocation points. This boundary is represented in the following equation (Tarafder et al.,2010):

$$\sum_{j=1}^N B_j \sigma_j + \sum_{j=1}^N C_j \mu_j + \Phi_\infty = const \quad (1.10)$$

## Influence coefficient calculation

This 3D panel method combine the source and doublet. That means, for every panel has a local source and doublet strength. And since we are using the Dirichlet boundary conditions and the equation (1.10) is not unique, we fix the strength source to get a set of equations with the doublet strengths as the unknowns.

$$\sigma_j = n \cdot Q_\infty \quad (1.11)$$

The boundary condition will reduce after setting the inner perturbation velocity equal to  $\Phi_\infty$  and will become (Tarafder et al.,2010):

$$\sum_{j=1}^N B_j \sigma_j + \sum_{j=1}^N C_j \mu_j = 0 \quad (1.12)$$

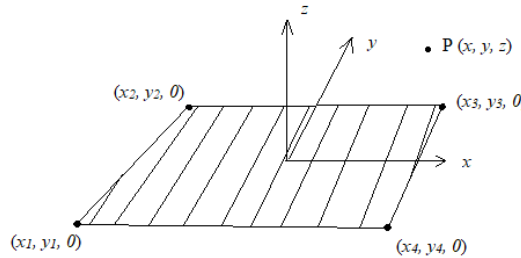


Figure 1.1. quadrilateral panel.

Regarding the figure (1.1), the panel vertex coordinates  $(x_1, x_2, x_3, x_4, y_1, y_2, y_3, y_4, z_1, z_2, z_3, z_4)$ , the  $x, y, z$  are the coordinates of influenced point  $\sigma$  and  $\mu$  source and vortex strength.

Considering a wake panel that is shed by an upper panel with a counter  $N$  and a lower panel with the counter  $l$  as shown in the figure (1.2). the equation of the first collocation point can be derived as (Katz & Plotkin, 2001):

$$C_{11}\mu_N + \dots + C_{1N}\mu_N + \dots + C_{1l}\mu_l + \dots + C_{1l}\mu_l + \sum_{p=1}^{N_w} C_{1p}\mu_p + \sum_{k=1}^N B_{1j}\sigma_j = 0 \quad (1.13)$$

Using the Kutta-condition on trailing edge

$$\mu_w = \mu_N - \mu_l \quad (1.14)$$

The previous equations are N equations with N+1 unknown. Kutta condition is used to add the N+1 equation for the N+1 unknown. Equation (1.14) will be as:

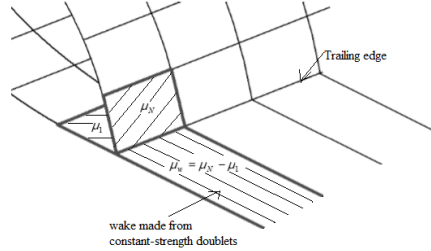


Figure 1.2. Kutta-condition at the trailing edge of the wing

$$C_{11}\mu_N + \dots + (C_{1N} + C_{1p})\mu_N + \dots + (C_{1l} - C_{1p})\mu_l + \dots + C_N\mu_N + \sum_{k=1}^N B_{1j}\sigma_j = 0 \quad (1.15)$$

This equation can be simplified into:

$$\sum_{k=1}^N A_{1j}\mu_j = -\sum_{k=1}^N B_{1j}\sigma_j \quad (1.16)$$

But if we have shedding from the trailing edge,  $A_{1j}$  will be equal to  $C_{1j}$  and if it's shedding,  $A_{1j}$  will be equal to  $C_{1j} \pm C_{1p}$ . In form of matrix, equation (1.17) will transform into:

$$\begin{pmatrix} a_{11} & a_{12} & \dots & a_{1N} \\ a_{12} & a_{22} & \dots & a_{2N} \\ a_{13} & a_{32} & \dots & a_{3N} \\ \vdots & \ddots & \vdots & \vdots \\ a_{N2} & a_{N2} & \dots & a_{NN} \end{pmatrix} \begin{pmatrix} \mu_1 \\ \mu_2 \\ \mu_3 \\ \vdots \\ \mu_N \end{pmatrix} = - \begin{pmatrix} b_{11} & b_{12} & \dots & b_{1N} \\ b_{12} & b_{22} & \dots & b_{2N} \\ b_{13} & b_{32} & \dots & b_{3N} \\ \vdots & \ddots & \vdots & \vdots \\ b_{N2} & b_{N2} & \dots & b_{NN} \end{pmatrix} \begin{pmatrix} \sigma_1 \\ \sigma_2 \\ \sigma_3 \\ \vdots \\ \sigma_N \end{pmatrix} \quad (1.17)$$

This matrix represents a set of N linear equations with N unknown. Note that  $a_{jj}=0.5$  on the diagonal except the trailing edge. Since the source strength is known then we can establish a right-hand side matrix, and this will be shown in the equation (1.18)

$$\begin{pmatrix} a_{11} & a_{12} & \dots & a_{1N} \\ a_{12} & a_{22} & \dots & a_{2N} \\ a_{13} & a_{32} & \dots & a_{3N} \\ \vdots & \ddots & \vdots & \vdots \\ a_{N2} & a_{N2} & \dots & a_{NN} \end{pmatrix} \begin{pmatrix} \mu_1 \\ \mu_2 \\ \mu_3 \\ \vdots \\ \mu_N \end{pmatrix} = \begin{pmatrix} RHS_1 \\ RHS_2 \\ RHS_3 \\ \vdots \\ RHS_N \end{pmatrix} \quad (1.18)$$